Micropore Size Estimation on Gas Separation Membranes: A Study in Experimental and Molecular Dynamics

Tomohisa Yoshioka, Masakoto Kanezashi, and Toshinori Tsuru
Dept. of Chemical Engineering, Hiroshima University, Higashi-Hiroshima 739-8527, Japan

DOI 10.1002/aic.13966
Published online December 27, 2012 in Wiley Online Library (wileyonlinelibrary.com).

The effect of the gas molecular size and its affinity to the pore surface on gas permeation properties through the ceramic membranes was studied by both the gas permeation experiments and gas permeation simulations using a nonequilibrium molecular dynamics (MD) technique. A modified gas permeation model equation based on the gas translation (GT) mechanism was presented. MD simulation revealed that the effective diffusion length in a micropore depended on the gas molecular size, and the pre-exponential coefficient of a modified GT model equation showed good correlation with the kinetic diameter of the gas molecules. Also presented is a simple method to estimate the mean pore size of microporous membranes. The estimated pore sizes were consistent with observed kinetic diameter dependencies of gas permeance for real silica membranes. The pore size of a Deca-Dodecasil 3R (DDR) zeolite membrane was also reasonably estimated at ~0.4 nm from the reported gas permeation data. © 2012 American Institute of Chemical Engineers *AIChE J,* 59: 2179–2194, 2013
Keywords: microporous membrane, gas permeation, micropore size, molecular dynamics

Introduction

The thermal and chemical stability of microporous ceramic membranes is reliable for use in gas separation processes under relatively high temperatures. The gas permeation and separation performance of microporous membranes depends largely on the pore size and the affinity to guest molecules. The diffusion of molecules in pores can be classified in a number of different regimes depending on the pore size.

Sol-gel or chemical vapor deposition (CVD)-derived silica membranes are known to have good hydrogen permselectivity in hydrogen separation from H_2/N_2 or H_2/CH_4 gas mixtures.[1–3] Silica membranes fabricated by the counter diffusion CVD method,[4] and sol-gel-derived Ni- or codoped silica membranes fired under hydrothermal condition at high temperatures,[5,6] have shown not only high hydrogen permselectivity but also good stability under steam reforming conditions up to 500°C. These amorphous silica-based hydrogen separation membranes are assumed to have very small pores due to silica polymer network voids of ~0.3 nm.[7] The gas permeation mechanisms through such small voids can be reliably studied using a solid vibration model.[8] Another model[3] that considers both the gas solubility (Shackelford et al. 1972)[9] of small voids based on statistical thermodynamics and diffusivity[10] can be used to explain the permeation properties of small gas molecules such as He, H_2, and Ne in microporous silica membranes.

However, to separate carbon dioxide and C2–C4 light hydrocarbons from exhaust gas, landfill gas, bio gas, and organic gas mixtures, a membrane pore of 0.3 nm is too small and a larger micropore of subnanoscale would be more effective because the molecular size of those gases is larger than that of both He and H_2. Amorphous silica membranes for CO_2/N_2 separation, with pore sizes of 0.3–0.4 nm that are well-controlled by the sol-gel technique are larger than the pores of hydrogen separation membranes.[11] Homogeneous microporous zeolite membranes such as ALPO-34[12,13] and DDR[14,15] with pore sizes ranging from 0.36 to 0.44 nm showed splendid CO_2 permselectivity in CO_2/CH_4 separation. CVD-derived membranes fabricated using silicon alkoxide with organic groups as a precursor have pores that are larger than those found in normal CVD silica membranes.[16] These membranes have good hydrogen permeability with porous structures that SF_6 and organic hydrides with sizes greater than 0.55 nm cannot permeate, which suggests they could be useful in membrane reactors for hydrogen production from organic hydrides as hydrogen carriers. We successfully prepared hybrid inorganic–organic silica-based membranes using the spacer sol-gel method and silicon alkoxide with a hydrocarbon group, $-(CH_2)_n-$ between Si atoms. These membranes showed excellent hydrogen permeance and high H_2/SF_6 selectivity for bis(triethoxysilyl)ethane (BTESE) membranes ($n = 2$).[17,18] Analysis by molecular simulation study revealed that BTESE membranes have greater pore sizes and looser microporous structures compared to normal pure silica membranes.[19] We considered the possibility that an $n = 1$, bis(triethoxysilyl)methane membrane might have permselectivity for C_3H_6 olefin gas from C_3H_6/C_3H_8 gas mixtures.[20] Gas permeation mechanisms through these types of larger subnanopores are recognized by gas translational (GT) diffusion,[8] surface diffusion, and Knudsen diffusion models.

The pore size characterization of microporous inorganic membranes that can be used for gas separation processes is of importance for the design of gas separation membranes as

Correspondence concerning this article should be addressed to T. Yoshioka at tom@hiroshima-u.ac.jp.

well as for the elucidation of gas permeation mechanisms. Obviously, the porous structures of powder samples of identical material can be well-characterized by an adsorption method. However, the *in situ* estimation of an effective micropore size for gas permeation and separation with membranes is not so straightforward and is not well-established. Positron annihilation lifetime spectroscopy[21] was recently developed and has potential as a novel characterization method for microporous media. However, limitations persist for a more widespread application to microporous membranes due to the lack of a systematic correlation of parameters with structural properties. Under the circumstances, the simplest *in situ* characterization method of microporous membranes has been to analyze the correlation between the gas permeance and the molecular size, by measuring permeance of gas molecules of different molecular sizes at high temperatures (150–300°C) where the effect of physical adsorption is possibly negligible. When a plot of gas permeance dependency on gas molecular size in a range of subnanoscale can be regarded as an accumulative pore-size distribution, it provides a very rough estimation of effective pore size for gas permeation. This so-called "probe gas permeation method" can be applied for characterization of microporous membranes of pore sizes smaller than 1 nm. The other method involves a "nano-perm-porometry (NPP)" technique.[22] A pore-size distribution ranging from 0.5 to 50 nm can be well-obtained from the partial pressure dependency of the noncondensable gas permeance of both condensable and noncondensable gas mixtures. The set partial pressures of condensable gases such as water and hexane can be theoretically converted to pore diameter using a Kelvin equation. Tsuru et al.[22,23] have reported that a pore size obtained by NPP has a good correlation with the permeation and separation performance of subnano and nanoporous membranes. According to their calculations, a pore size of 0.5 nm could be estimated by NPP. However, taking into account the applicable limitations of the Kelvin equation makes questionable the absolute values of estimated pore sizes of less than 1 nm. To examine the relationship between micropore size and gas permeation characteristics, Lee et al.[24] calculated normalized Knudsen-based permeance (NKP), which is an experimentally observed gas permeance at a constant temperature for different molecular sizes of gases divided by an ideal Knudsen permeance of each gas expected from He permeance according to the molecular weight ratio. The NKP was plotted against molecular size, and a simple *in situ* estimation method of mean pore size was proposed, with the assumption that the gas permeance of a subnanoscale pore was proportional to a cubic of the mean effective diffusion length of the pore, which depended on the gas molecular size, and was also inversely proportional to the squared root of the gas molecular weight as the Knudsen diffusion. This NKP plot is a simple method to estimate an effective mean pore size for gas permeation from the molecular size dependency of gas permeance under a constant temperature in the case of a small temperature dependency of permeance due to the small interaction between a membrane and gas molecules where both the adsorption and activation energy of gas molecules can be reasonably negligible. However, the membranes which have a large affinity with CO_2 or light hydrocarbons and on which a so-called surface diffusion-like temperature dependency of gas permeance can be observed, such as normal pure silica membranes and DDR zeolite membranes, are not suitable for the characterization of porous structures using the NKP-plot method.

The objective of the present work was to present a simple estimation method for the effective mean pore size and porous structures of microporous inorganic membranes by using a modified GT model that took into consideration the size of gas molecules and the affinity with a membrane. The applicability of the method and the adequacy of the gas permeation model were examined through studies of the gas permeation properties of real silica membranes, ideal virtual silica membranes using molecular dynamics (MD) simulation, and a DDR zeolite membrane, as reported in the literature.

Gas Permeation Model

In general, gas permeation mechanisms of microporous membranes depend on porous structures such as pore size and pore shape, physical chemical properties of permeating molecules such as molecular size, molecular shape, and interactions with membranes, and external operating conditions such as temperature and pressure. For large pore diameters, usually called macropores on the order of 1 μm or larger, collisions between the molecules occur much more frequently than collisions with the wall, and viscous flow with molecular diffusion is the dominant mechanism. In this case, the separation of gas mixtures by a membrane is impossible. The number of collisions with the wall increases as the size of the pores decreases until it finally becomes smaller than the mean free path of the gas molecules. At this point, Knudsen diffusion takes over the transport mechanisms of permeating gas molecules. When gas transport by the Knudsen regime diffusion in a micropore occurs under the chemical potential gradient as a driving force, with the assumption of an ideal gas in the bulk gas phase, the diffusion flux, J in the direction of permeation, z can be given by Eq. 1,[25] where μ is the chemical potential, B is the mobility, and c is the concentration in a micropore (equivalent to gas density or the adsorbed amount in the pore)

$$J = -Bc\frac{d\mu}{dz} = -D'\frac{d\ln p}{d\ln c}\frac{dc}{dp}\frac{dp}{dz} \tag{1}$$

D' is a thermodynamic corrected diffusion coefficient, which satisfies the "Darken equation," Eq. 2, for the relationship with the Fick's diffusion coefficient, D

$$D = D'\frac{d\ln p}{d\ln c} \tag{2}$$

The permeability, $P = JL/\Delta p$ can be obtained by integrating Eq. 1 for pressure from the feed side to the permeate side, where L is the length of the pore

$$P = \frac{JL}{\Delta p} = -\frac{\int_{p_1}^{p_2} D'\frac{d\ln p}{d\ln c}\frac{dc}{dp}dp}{p_1 - p_2} \tag{3}$$

Equation 3 indicates that the permeability can be estimated from the diffusivity in a micropore, D', and the relationship between the bulk gas-phase pressure, p, and the concentration in a micropore, c, which is an equilibrated adsorbability. When the interaction acting on a permeating molecule inside a pore space is negligible, as with the bulk gas phase, when the relationship for $c = p/RT$ is satisfied, the permeability is derived as in Eq. 6 from Eq. 3 using the following Eqs. (4) and (5) under a constant temperature, T

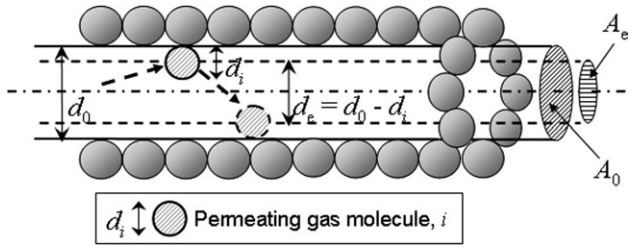

Figure 1. Schematic drawing of the diffusion of a gas molecule with the determinate size of d_i in a micropore.

$$\frac{dc}{dp} = \frac{1}{RT} \tag{4}$$

$$\frac{d\ln c}{d\ln p} = 1 \tag{5}$$

$$P = -\frac{\int_{p_1}^{p_2} \frac{D'}{RT} dp}{p_1 - p_2} = \frac{D'}{RT} \tag{6}$$

With the assumptions that the pore diameter is small and the concentration is low enough so that the number of collisions of a permeating molecule with the pore wall occurs much more frequently than collisions with the molecules, the so-called Knudsen diffusion is the dominant diffusion mechanism of molecular transport within a pore, and D' is given as a product of the mean velocity of a molecule, the effective pore diameter d_e, and the moving probability in a 3-dimensional (3-D) space ρ[25]

$$D' = \rho d_e \sqrt{\frac{8RT}{\pi M}} \tag{7}$$

By Knudsen diffusion, the ideal permeability per cross-sectional area of one pore is given by Eq. 8

$$P_K = \frac{D'}{RT} = \rho d_e \sqrt{\frac{8}{\pi MRT}} \tag{8}$$

Therefore, the Knudsen permeance P_{KL}, that was experimentally observed for a membrane, composed of micropores with homogeneous sizes, with the thickness of the active separation layer, L, the porosity, ε, and the tortuosity, τ, is expressed by Eq. 9

$$P_{KL} = \frac{P_K}{L}\frac{\varepsilon}{\tau} = \frac{\rho \varepsilon d_e}{\tau L}\sqrt{\frac{8}{\pi MRT}} \tag{9}$$

Because a potentially permeating molecule is, in reality, not a simple mass point, but rather is an object of finite size, the probability that said molecule will move in the direction of permeation is given by the product of (1) the ratio of the effective cross-sectional area of a pore A_e, over the true cross-sectional area of the pore A_0, (2) an exponential term for the activation energy that is needed to overcome the diffusion barrier in a micropore, and (3) random factor 1/3 in a 3-D space[24]

$$\rho = \frac{1}{3}\frac{A_e}{A_0}\exp\left(-\frac{E_{act,i}}{RT}\right) \tag{10}$$

For simplicity, as shown in Figure 1, we assumed that the shape of the cross-section of a pore was the diameter d_0, of a circle and that an approximately spherical molecule with diameter d_i would diffuse through the pore. The effective diffusion length of a pore is reduced by the molecular size of a permeating molecule due to its finite volume, and the shape of an effective pore cross-section is supposed to be a circle with a diameter $d_e = d_0 - d_i$.[24] Therefore

$$A_0 = \frac{\pi}{4}d_0^2 \tag{11}$$

$$A_e = \frac{\pi}{4}d_e^2 = \frac{\pi}{4}(d_0 - d_i)^2 \tag{12}$$

The idea of effective diffusion space depending on permeant size is a universal concept that is seen in descriptions of Ferry's equation[26] for the analysis of solute permeation in ultrafiltration, and in Xiao's model[8] for gas diffusion considering the ratio of the channel diameter to the gas molecular diameter. The porosity, ε, is defined by the membrane area A_m, the number of pores N_P with pore diameters of d_0 on the membrane, and A_0, as shown by Eq. 13

$$\varepsilon = \frac{A_0 N_P}{A_m} \tag{13}$$

Therefore

$$P_{KL} = \frac{N_P}{6\tau A_m L}\sqrt{\frac{2\pi}{MRT}}(d_0 - d_i)^3 \exp\left(-\frac{E_{act,i}}{RT}\right) = \frac{k_0}{\sqrt{MRT}}(d_0 - d_i)^3 \exp\left(-\frac{E_{act,i}}{RT}\right) \tag{14}$$

where, k_0 is a constant that depends only on the membrane porous structures and is independent of the permeating gas species, as given by Eq. 15

$$k_0 = \frac{N_P\sqrt{2\pi}}{6\tau A_m L} \tag{15}$$

Equation 10 describes the diffusion probability of a gas molecule within a micropore in 3-D over the diffusion barrier in a Knudsen diffusion regime. This description of gas diffusion probability was adopted in the GT model originally proposed by Xiao and Wei[8] and Shelekhin et al.[25] The only change, and the novel point of our model, reported in the present and previous work[20,24] by our group was that the effective diffusion length in a micropore was considered instead of the actual pore size.

When a relatively weak interaction such as van der Waals dispersion force works on the permeating molecules, a Henry type of weak adsorption can occur, and the molecular density in the pore increases in proportion to the pressure of the bulk gas phase. The extent of this interaction depends on the species of the permeating gas and differs when the permeating molecular type is different even when the permeation is through an identical pore. When the interaction energy is on the order of several kJ/mol, the concentration in a micropore, c, is severalfold greater than that of the bulk gas phase c_b, according to the Boltzmann distribution theorem

$$\frac{c}{c_b} = \exp\left(-\frac{E_{att,i}}{RT}\right) \tag{16}$$

For example, if the potential in a pore $E_{att,i}$, the interaction affect on a permeating molecule by the pore wall, is

-5 kJ/mol, the c/c_b would be equal to 7.4 at 300 K, and the number density of molecules in a micropore would be about 0.2 nm^{-3} if the feed side pressure was 105 kPa. The frequency of collisions among permeating molecules under the experimental temperature and pressure conditions of the Knudsen regime was not as high as that against a pore surface. Therefore, when the gas-phase pressure is several atmospheres, the extent of concentration in a pore cannot be regarded as a normal adsorption with a phase transition from gas to liquid. It would be reasonable to suppose that the guest molecules are still being transported in the gas phase, and that each molecule diffuses independently in a micropore. In this case, the relationship between the gas-phase pressure, p, and concentration in a pore, c, would be as follows[11]

$$c = \frac{p}{RT}\exp\left(-\frac{E_{\mathrm{att},i}}{RT}\right) \tag{17}$$

And therefore, a constant temperature, T, would result in the following

$$\frac{dc}{dp} = \frac{1}{RT}\exp\left(-\frac{E_{\mathrm{att},i}}{RT}\right) \tag{18}$$

This is also the case for diffusion in a micropore when the gas state diffusivity, D', is reasonably given by Eq. 7, then the gas permeability and permeance equations corresponding to Eqs. (8) and (14) are as follows

$$P_{\mathrm{cK}} = \frac{D'}{RT}\exp\left(-\frac{E_{\mathrm{att},i}}{RT}\right) = \rho d_e\sqrt{\frac{8}{\pi MRT}}\exp\left(-\frac{E_{\mathrm{att},i}}{RT}\right) \tag{19}$$

$$P_{\mathrm{cKL}} = \frac{P_{\mathrm{cK}}}{L}\frac{\varepsilon}{\tau} = \frac{\rho\varepsilon d_e}{\tau L}\sqrt{\frac{8}{\pi MRT}}\exp\left(-\frac{E_{\mathrm{att},i}}{RT}\right) = P_{\mathrm{KL}}\exp\left(-\frac{E_{\mathrm{att},i}}{RT}\right) \tag{20}$$

where P_{cKL} is the Knudsen permeance of gas molecules that are concentrated by the attractive nature of the potential field of the pore wall. When using Eq. 10 to account for the probability of transportation in the direction of permeation, we obtain Eq. 21

$$P_{\mathrm{cKL}} = \frac{k_0}{\sqrt{MRT}}(d_0 - d_i)^3\exp\left(-\frac{E_{\mathrm{act},i} + E_{\mathrm{att},i}}{RT}\right) \tag{21}$$

These types of gas permeation models have been reported previously. The GT diffusion model[8] is described as a combination of activated diffusion by jumping from cage to cage of zeolite and molecular diffusion by translational movement within a cage pore. The energy of the exponential term is successfully treated as the summation of activation energy and adsorption energy.[25] Burggraaf[27] called this combination of GT and SD (surface diffusion) mechanisms "surface diffusion enhanced micropore permeation." In the case of gas-state permeation under conditions of high temperature or low pressure, it is called "Concentrated-Knudsen permeation." Our proposed model adopts the main concepts of those models and additionally considers the effective diffusion length. Equation (21) provides a more detailed description of the gas permeation model equation by considering activation energy and adsorption energy, as well as gas molecular size. The value of $E_{\mathrm{P},i}$ can be easily estimated as an apparent activation energy ($E_{\mathrm{P},i} > 0$), or as an apparent adsorption energy ($E_{\mathrm{P},i} < 0$) by fitting Eq. 22 to the temperature dependency of gas permeance data to obtain adjusting parameters $k_{0,i}$ and $E_{\mathrm{P},i}$, which are defined as $k_{0,i} = k_0(d_0 - d_i)^3$ and $E_{\mathrm{P},i} = E_{\mathrm{act},i} + E_{\mathrm{att},i}$

$$P_{\mathrm{cKL}} = \frac{k_{0,i}}{\sqrt{MRT}}\exp\left(-\frac{E_{\mathrm{P},i}}{RT}\right) \tag{22}$$

The derivation of Eq. 22 makes it obvious that the equation represents the normal ideal Knudsen diffusion for a case of $d_i = 0$ and $E_{\mathrm{P,i}} = 0$, and the ideal Knudsen permeance, P_{iKL}, would be as follows

$$P_{\mathrm{iKL}} = \frac{k_0 d_0^3}{\sqrt{MRT}} \tag{23}$$

In reality, the activation energy for transportation through amorphous silica network voids is so large that it cannot be ignored ($E_{\mathrm{act},i} > -E_{\mathrm{att},i}$), and the apparent activation diffusion behavior of gases is $E_{\mathrm{P},i} > 0$. On the contrary, for larger zeolite crystalline pores and for the aggregate pores of crystalline or colloidal boundaries where the diffusion barrier is relatively small, the attractive interaction of permeating gases with a pore wall is a dominant factor for the formation of gas permeation characteristics ($E_{\mathrm{act},i} < -E_{\mathrm{att},i}$), and gas permeation behavior that is based on so-called "surface diffusion" can be observed ($E_{\mathrm{P},i} < 0$). We previously presented a simple method for the pore size estimation for membrane micropores of ~0.5 nm using gas permeance data by considering the effect of gas molecular size on the molecular diffusion in a micropore.[24] In a previous paper, the following assumptions were adopted for Eq. 21.

1. All gas species permeate through an identical size of pore, which equates to the mean pore size.
2. The difference in activation energy for transportation through pores that range from several angstroms to 1 nm is reasonably negligible, and is independent of gas species.
3. When inorganic gas permeates a membrane pore at temperatures that range from 200 to 300°C, the gas concentration that results from the attractive interaction with the pore wall can be ignored.

The relative gas permeance (NKP) f_{NKP}, which is a corrected gas permeance normalized by standard gas permeance P_S, that considers the contribution of molar weight, can be easily calculated as a function of gas molecular size d_i, by measuring the gas permeances of several gas species at a given constant temperature

$$f_{\mathrm{NKP}} = \frac{P_i}{P_S}\sqrt{\frac{M_i}{M_S}} = \frac{(d_0 - d_i)^3\exp\left(-\frac{E_{\mathrm{act},i}+E_{\mathrm{att},i}}{RT}\right)}{(d_0 - d_S)^3\exp\left(-\frac{E_{\mathrm{act,S}}+E_{\mathrm{att,S}}}{RT}\right)} \approx \left(\frac{1-\frac{d_i}{d_0}}{1-\frac{d_S}{d_0}}\right)^3 \tag{24}$$

Under the limiting conditions of $d_S < d_i < d_0$, Eq. 24 fits well with the data of f vs. d_i by using d_0 as an adjusting parameter, and the mean effective pore size for gas permeation of the membrane d_0, can be estimated. The permeance and molecular size of He, the smallest of all the molecules, would be suitable for P_S and d_S, respectively. For zeolite membranes and silica membranes, however, the gas permeation data of CO_2 and light hydrocarbons show a surface diffusion-like behavior, which is due to a larger adsorption energy,[27] and,

therefore, the above assumptions (2) and (3) are not reasonable, and Eq. 24 is not applicable for the estimation of pore size for those microporous membranes. In this case, Eq. 24 should be interpreted in its strict form, which is Eq. 25

$$f_{\mathrm{NKP}} = \frac{P_i}{P_{\mathrm{S}}}\sqrt{\frac{M_i}{M_{\mathrm{S}}}} = \frac{(d_0 - d_i)^3 \exp\left(-\frac{E_{\mathrm{act},i}+E_{\mathrm{att},i}}{RT}\right)}{(d_0 - d_{\mathrm{S}})^3 \exp\left(-\frac{E_{\mathrm{act,S}}+E_{\mathrm{att,S}}}{RT}\right)} = \left(\frac{1-\frac{d_i}{d_0}}{1-\frac{d_{\mathrm{S}}}{d_0}}\right)^3 \exp\left(-\frac{E_{\mathrm{P},i} - E_{\mathrm{P,S}}}{RT}\right) \quad (25)$$

f_{NKP} should also be corrected using the value of $E_{\mathrm{P},i}$ as in Eq. 26, where f_{mNKP} is referred to as a modified NKP

$$f_{\mathrm{mNKP}} = \frac{P_i}{P_{\mathrm{S}}}\sqrt{\frac{M_i}{M_{\mathrm{S}}}}\exp\left(-\frac{E_{\mathrm{P,S}} - E_{\mathrm{P},i}}{RT}\right) = \left(\frac{1-\frac{d_i}{d_0}}{1-\frac{d_{\mathrm{S}}}{d_0}}\right)^3 \quad (26)$$

It is obvious from Eq. 26 that in the case of gas permeation by ideal Knudsen diffusion, $d_{\mathrm{S}} = d_i = 0$ and $E_{\mathrm{P,S}} = E_{\mathrm{P},i} = 0$, the relative ideal permeance of the mass point which is corrected by molar weight, f_{iNKP} (Ideal NKP) is equal to the unity and is independent of both the gas species and the pore size

$$f_{\mathrm{iNKP}} = \frac{P_{\mathrm{iKL},i}}{P_{\mathrm{iKL,S}}}\sqrt{\frac{M_i}{M_{\mathrm{S}}}} = \sqrt{\frac{M_{\mathrm{S}}}{M_i}}\sqrt{\frac{M_i}{M_{\mathrm{S}}}} = 1 \quad (27)$$

Because the value of f_{mNKP} includes the effect of molar weight and the interaction with the pore wall on gas permeance, a deviation of f_{mNKP} from 1 would reflect the effective mean free path in a micropore that depends on real gas molecular size. It is not easy to obtain each value of $E_{\mathrm{act},i}$ and $E_{\mathrm{att},i}$ separately from gas permeance measurements. However, the summation $E_{\mathrm{P},i}$, can be easily estimated from the temperature dependency of gas permeance using Eq. 22. In addition $k_{0,i}$ is also obtained as another adjustable parameter, as is $E_{\mathrm{P},i}$.

According to the equation $k_{0,i} = k_0(d_0 - d_i)$,[3] the following would be true

$$\sqrt[3]{k_{0,i}} = \sqrt[3]{k_0}d_0 - \sqrt[3]{k_0}d_i \quad (28)$$

Therefore, if the model is correct, we can expect a linear relationship between d_i and ${k_{0,i}}^{1/3}$ with a slope of $-{k_0}^{1/3}$ and an intercept of $-{k_0}^{1/3}d_0$. From the figure showing the plot of ${k_{0,i}}^{1/3}$ against d_i, both the value of d_0 as an effective pore size for gas permeation and the structural parameter k_0 can be easily estimated. The validity of the above ''Concentrated-Knudsen permeation model'' was examined through the experimental study of gas permeation properties for amorphous silica membranes, molecular dynamic simulations of gas permeation for virtual silica membranes, and application to reported gas permeation data for a DDR zeolite membrane.

In general, the structure of the micropores, which consists of a network of silica polymers, is not straight-shaped and cylindrical. Polymer networks made up of silica membrane with H_2/N_2 selectivity are dominant in the field of gas separation. Therefore, the above cylindrical pore model is not applicable to the analysis of gas permeation properties on amorphous silica membranes. The silica membranes prepared in this study, however, did not display the excellent molecular sieving performance of a hydrogen separation membrane, as shown later. Those membranes were more effective for the selective permeation of molecules with sizes that ranged from 0.4 to 1.0 nm, which is slightly larger than that of hydrogen (0.289 nm). The effective pores on those membranes were the aggregated micropores that remained from the sintering step of the sol-gel-derived membrane preparation process, and the small voids of 0.3 nm that originated from the network structure of the silica polymer where the activated diffusion behavior was observed[7] were not as effective. Because the size of the silica polymer colloid that is currently used to coat the top layer of silica membranes is at no more than 10 nm,[11] we believed it was appropriate to assume that the fundamental unit of a micropore would be a cylindrical pore several nanometers long. Such small pores are supposed to be connected randomly in 3-D so as to form an actual separation layer of around 100–500 nm in thickness with crooked pores. The effect of this crookedness was taken into consideration in the gas permeation model as a tortuosity coefficient.

Experimental and Simulation

For this study, we used previously established results of sol-gel microporous silica-based membranes with a pore size controlled to less than 1 nm and were almost pinhole-free for hydrogen, CO_2, and PV separation of an aqueous solution of alcohol. Those membranes can be suitably prepared by regulating the coating times and colloidal sizes of sols.[11] For examination of the dependency of gas permeation properties on pore size taking into account pore wall interactions with micropores ranging from 0.3 to 1 nm, it is preferable to use membranes made of identical materials with different pore sizes and with no specific interactions such as chemical adsorption. To obtain suitable pores in the 0.3–1 nm range, sol-gel-derived amorphous silica membranes with nanocolloid-oriented aggregate micropores formed in coating and calcination processes are good candidates. For real silica membranes, however, despite gas separation characteristics that include a narrow pore-size distribution, the effect of the slight nonuniformity of pore size on gas permeance cannot be excluded from validation of the pore size estimation when using Eq. 26 that assumes a homogeneous porous structure.

We also adopted a nonequilibrium MD technique for the gas permeation simulation of ideal virtual silica membranes with given pore sizes d_0. One of the advantages of using molecular simulation is that it enables an essential validation of Eq. 26 as the ''value'' for the pore size is known, and it is free from pinholes and a pore-size distribution. Another merit is that the effective diffusion length of a micropore can be known on a molecular scale, which is also useful for examination of Eq. 26.

Preparation of silica colloid sols and silica membranes

Silica colloidal sols and silica membranes were prepared using a previously reported procedure.[11] The silica colloidal-sol solutions were prepared through hydrolysis for 1 h at room-temperature, polymerization, and condensation for about 10 h at the boiling point of tetraethoxysilane (TEOS, $Si(OC_2H_5)$) aqueous solutions with a small amount of HNO_3 as the catalyst at 0.5–2.0 wt % of TEOS. The particle sizes of silica colloidal sols could be well-controlled in sizes that ranged from ~3 to 100 nm by adjusting the concentration of the starting TEOS aqueous solution.[11] Several different colloidal sizes of sols were prepared by changing the TEOS concentration, after which they were coated onto a porous

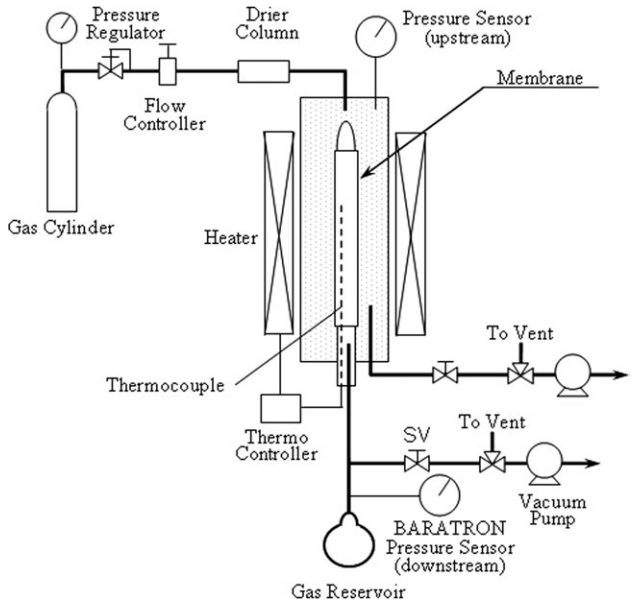

Figure 2. Schematic drawing of the experimental apparatus for gas permeance measurements.

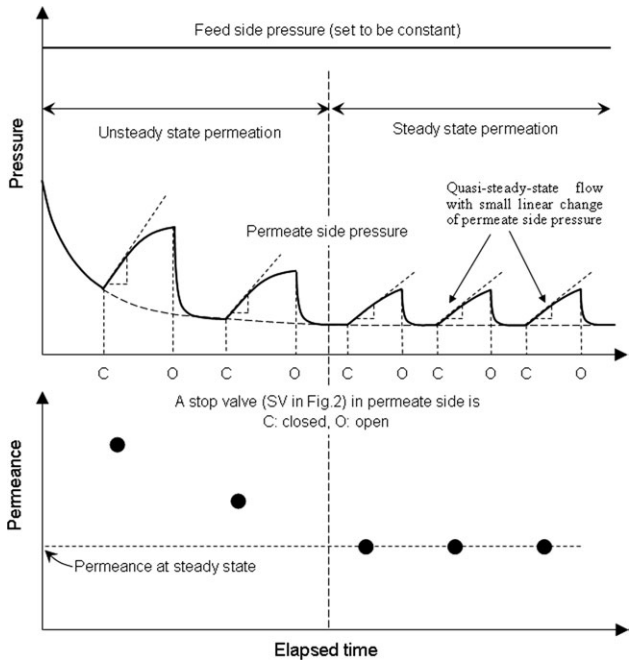

Figure 3. Schematic image of the time course of observed pressure and calculated permeance during a gas permeation measurement.

a-alumina support in decreasing order of colloidal size to construct asymmetric membranes. The membranes were calcined at 500°C in air for 15 min after every sol coating operation. We prepared three different microporous silica membranes, M-1, M-2, and M-3, for this study, all of which were applicable to gas separation. The intermediate layers of all membranes used in this work were prepared by using 2.0–1.0 wt % sols. The top layers of these membranes were primarily formed by coating 0.5 wt % (M-1 and M2) and 1.0 wt % (M-3) silica sols with different coating times for M-1, M-2, and M-3, respectively.

Gas permeation experiments

Figure 2 shows the experimental apparatus that was used for the gas permeance measurements—a cylindrical membrane module mounted in a temperature-controlled cell. The upstream pressure was controlled either at 105 kPa (He, H_2, O_2, N_2, CH_4, SF_6) or 2.7–13.3 kPa (CO_2, C_3H_8) by a pressure regulator and mass flow-controller, whereas the downstream portion of the membrane was evacuated by a vacuum pump. For measurements of CO_2 and hydrocarbon permeance, evacuated pressure conditions were adopted for the feed side to insure gas-state permeation under a Henry-type low-adsorption regime. The flow rate (mol s^{-1}) of the permeant was calculated from the volume of the gas reservoir and the rate of pressure increase after the downstream line to the vacuum pump was closed (quasisteady-state flow method), then the flow rate was converted to permeance (mol m^{-2} s^{-2} Pa) when it was divided by the membrane surface area and the pressure drop across a membrane. In general, it takes time to achieve steady-state permeation after gas is fed to a membrane module, particularly for gases that have a large affinity with membranes such as carbon dioxide and sulfur hexafluoride. Therefore, before measuring gas permeance, each gas was fed to the gas permeation equipment and allowed to permeate the membrane for sufficient amount of time (longer than 1 h) to achieve steady-state permeation. During this 1 h, a series of operations that included the closing of a stop valve in the permeate side, calculation of the permeance from the rate of linear increase in the permeate side pressure, and the opening of a stop valve in the permeate side (resumption of permeation) were repeated many times over, and we confirmed that steady-state permeation was completed by checking that the observed permeance converged to a constant value along with time, as schematically shown in Figure 3. Therefore, we can assure that all the values of permeance shown in this work are those of constant permeance at steady state.

Gas permeation experiments were performed in temperature that ranged from 35 to 300°C. All gas permeation measurements were conducted under conditions that used a decreasing order of temperature after pretreatment of the He flow at 300°C for fresh membranes immediately following fabrication. The gas species used for the gas permeance measurements and their kinetic diameters are summarized in Table 1.

MD simulation

The virtual membrane was an amorphous silica composed of silicon and oxygen, and virtual LJ particles of six spherical symmetric gas species, He, Ne, Ar, CH_4, Xe, SF_6, were assigned as permeants. The reasons why those molecules were adopted in this work were followings; (1) the real shape of those molecules is symmetric and they can be

Table 1. Kinetic diameter of gas molecules[28]

i	d_i (nm)
He	0.26
H_2	0.289
CO_2	0.33
O_2	0.346
N_2	0.364
CO	0.376
CH_4	0.38
C_3H_8	0.43
iso—C_4H_{10}	0.50
SF_6	0.55

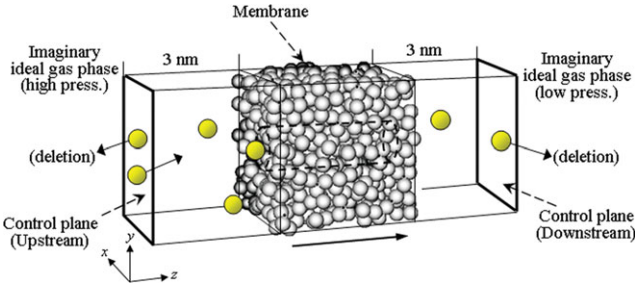

Figure 4. Schematic image of a DCP-NEMD simulation cell.

[Color figure can be viewed in the online issue, which is available at wileyonlinelibrary.com]

reasonably assumed to be represented with Lennard-Jones particles, (2) those molecules have different molecular sizes each other in subnanoscale, and (3) those molecules can have different interaction with the pore surface. Therefore, we considered that they were suitable for examination of the validity of the gas permeation model and micropore size estimation method presented in this work. A modified Born–Mayer–Huggins two-body potential and a Stillinger–Weber three-body potential were used to prepare the amorphous silica structures.[7,29] A well-known Lennard-Jones 12-6 potential (Eq. 29) was used to calculate the interactions between the permeating molecules and the oxygen atoms on silica membranes. The potential functions and parameters that were used for the construction of the silica structure were previously outlined by Yoshioka et al.[7]

$$E(r_{ij}) = 4\varepsilon_{ij}\left[\left(\frac{\sigma_{ij}}{r_{ij}}\right)^{12} - \left(\frac{\sigma_{ij}}{r_{ij}}\right)^{6}\right] \tag{29}$$

Virtual silica membranes were prepared using a Melt-Quench procedure.[29] At the starting point, 1024 oxygen atoms and 512 silicon atoms were configured as a β-cristobalite crystalline structure with a density of 2.2 g cm^{-3}. After the system was melted at 6000 K, it was quenched to 300 K at an average cooling rate of 10^{13} K/s to obtain a bulk amorphous silica structure. The details of the preparation procedure for virtual silica membranes have been described elsewhere.[30,31] The dimensions of the resultant MD silica membrane unit were $2.85 \times 2.85 \times 2.85$ nm^3 of length for the x-, y-, and z-directions. Three different virtual membrane units (VM-1, VM-2, and VM-3), each with a different size of cylindrical penetrating pore, were prepared by digging into the unit to create a cylindrical pore in the z direction. Both the silicon and oxygen atoms, with centers located within the circle of a given diameter in the x-y plane, were removed. Through the digging operations, 93, 171, and 273 atoms were removed from the interior of the body to form pores of 0.8, 1.0, and 1.3 nm in diameter, respectively. After the pore digging, the system was again relaxed at 300 K for 50 ps.

Gas permeation simulations with a constant pressure gradient across a membrane under a constant temperature were conducted using the dual-control plane nonequilibrium MD (DCP-NEMD) method.[31] Two control planes were settled at a sufficient distance from the membrane surface on the feed and permeate side, respectively, and gas molecules were either generated on the feed side or deleted from the permeate side plane to maintain a constant pressure drop. Figure 4 shows the schematic image of a DCP-NEMD simulation cell. Gas molecules were introduced to the simulation cell from the CP in the feed side at a frequency, f, that was given by Eq. 30 at a set temperature and feed-side pressure, where S was the area of the CP

$$f = \frac{pS}{(2\pi m k_B T)^{0.5}} \tag{30}$$

One molecule was sure to be generated during each time interval of $1/f$ [s], but the time was randomly chosen during f. Those molecules that reached the CPs after rebounding on the membrane surface or permeating through the membrane were unconditionally deleted. The initial velocity of a newly generated molecule on the CP was given based on the kinetic theory of an ideal gas to satisfy the appropriate velocity distribution at a set temperature.

In the nonequilibrium MD calculation used in this work, the bulk gaseous phase was assumed to be the ideal gas phase of single gas. This approximation is not so unreasonable for a gas phase consisting of Lennard-Jones particles at 0.5 MPa and 300–800 K. For ideal gases, the chemical potential in a "Control Volume" is decided only by the pressure and temperature of the gas phase, and the frequency, f [1/s], for molecules to move in one way only through a plane in a gas phase can be determined by Eq. 30 according to the kinetic theory of ideal gases.[7,31] By generating a molecule on a "Control Plane" toward an MD simulation cell by the frequency of Eq. 30, the MD cell is set up to be in pressure and thermal equilibrium with an imaginary ideal gas phase outside the CP. In this case, a grand canonical Monte Carlo calculation within a "Control Volume" used in usual DCV-NEMD simulation is omissible.[32] Ford and Glandt[33] had already adopted "the plane method" to produce gas-phase molecules for investigating the surface barrier effect of the penetration of dilute gas molecules through a pore mouth. In their work, gas molecules were randomly assigned initial x and y positions in the plane settled at $z = 3.5\sigma$, the distance from the pore mouth. The initial velocities of gas molecules were chosen from a subset of the Maxwell–Boltzmann distribution that included only negative z velocities at a specified temperature. This molecular generating technique is simple and has been used.

For pressure control on a control plain, the frequency of the generation of molecules, as defined by Eq. 30, and the direction of the molecule which passes CP are very important. A molecule is generated only toward the direction of a MD cell (membrane), and a molecule which comes from the membrane is deleted unconditionally (compulsorily) on each CP. At the beginning of the calculation, as the number of molecules coming from two CPs at a certain time period is greater than that of molecules leaving from the MD cell toward the CPs and is deleted from them, the number of molecules in the MD cell increases with simulation time. At a steady state, however, on each CP of a feed side and a permeate side of the MD cell, the frequency of generation of molecules equals to the frequency that molecules pass the CP from the MD cell to an imaginary gas phase. Therefore, the number of molecules in the MD simulation cell is kept nearly constant at a steady state. We can check whether the system reached a steady state or not by counting the number of molecules in the MD cell along with time[31]. We can also determine whether the system has reached a steady state or not by checking the change of permeance along with time. A steady-state permeation state was completed after a

Table 2. Lennard-Jones Potential Parameters

i	σ_i (nm)	ε_i/k_B (K)
b-O	0.27	230
nb-O	0.30	230
He	0.26	10.22
Ne	0.282	32.8
Ar	0.3542	93.3
CH_4	0.38	148
Xe	0.41	221
SF_6	0.5128	222.1

calculation of 10 ns at longest, and we could obtain a reliable value of permeance using the number of permeate molecules.

If one want to set the pressure in the permeate side to a value of more than zero, molecules should be generated on a CP in the permeate side toward the MD cell by the frequency of Eq. 30 as well. In this case, one should substitute a pressure smaller than the pressure of the feed side for a variable, p, as in Eq. 30.

Permeating gas molecules were affected by both the interactions from other gas molecules and oxygen atoms on the pore wall, while the interactions with silicon atoms were neglected due to their small polarizability.[34] The Lorentz–Berthelot mixing rules[35] were used to estimate intermolecular potential parameters between pairs of nonidentical molecules (ij) from those between pairs of identical molecules (ii and jj). The Lennard-Jones potential parameters used in this study are summarized in Table 2. The notation for b-O (bridging oxygen) indicates the parameters for oxygen atoms in siloxane bonding, and nb-O (nonbridging oxygen) represents the oxygen in a silanol group that would be terminated by an imaginary hydrogen atom. The thermal vibration of silicon and oxygen atoms in the membrane also was taken into account along with the translational movements of permeating molecules in our simulations. The temperature of the system was controlled by assigning only the initial velocity of the permeating molecules based on the kinetic theory of gases and the periodical velocity scaling of the membrane constituting atoms. No other artificial operations for the kinetic energy of a permeating molecule were used. One MD time step was 1 fs, and the fifth-order Gear predictor-corrector algorithm was adopted to solve the Newtonian equation of motion and to obtain successive locations and velocity data for each molecule.

Gas permeances (mol m^{-2} s^{-1} Pa^{-1}) were calculated from the number of permeated molecules during a certain period at steady state primarily under the conditions of 0.5 MPa upstream pressure and 0 downstream pressure. In the case of Xe and SF_6 gas permeation, there was a relatively large interaction with the pore surface, and the upstream side pressure was set at the lower pressure of 0.1 MPa to prevent deviation from the Henry-type adsorption regime. Whether or not the system had reached a steady permeation state was confirmed by checking the slope of the accumulated number of permeated molecules plotted against time. A good linearity of the slope meant that the permeation rate was stable and the system could be assumed to have reached a steady state. For example, a SF_6 permeation rate at 800 K in VM-1, the smallest permeability that was observed for all our simulations, was calculated from the linear slope of several hundreds of accumulated permeated molecules at 100–540 ns (100,000,000–500,000,000 steps), and to calculate the CH_4 permeation rate at 300 K in VM-3, the largest permeability, a time of 5–35 ns (5,000,000-35,000,000 steps), was adopted. Gas permeances were calculated at temperatures of 300–800 K, and temperature dependency of permeance was examined using Eq. 22.

The apparent thickness of real silica membranes is several hundreds of nanometers, and is greater than that of the virtual silica membranes by a factor of 100. The effective length of the neck portion of the pores of real silica membranes, however, is possibly shorter than the apparent thickness. Despite the fact that the MD simulation cell size and the number of molecules were much smaller and less than that of real systems, the simulated gas permeation properties[7,30] showed good qualitative agreement with the experimental results for real porous silica membranes.[11] Therefore, this simulation system is reasonable for a study of the correlation between gas permeation phenomena within micropores and for a reasonable range of micropore sizes.

Results and Discussion

Real amorphous silica membranes

Figure 5 shows the molecular kinetic diameter dependencies of gas permeance observed for real silica membranes, M-1, M-2, and M-3, at 200°C. Each value of gas permeance was normalized by He permeance. He permeances of M-1, 2, and 3 were 1.11×10^{-6}, 2.10×10^{-6}, and 2.10×10^{-6} for units of (mol m^{-2} s Pa^{-1}), respectively. With respect to M-1, the gas permeance of large molecules such as C_3H_8, iso-C_4H_{10}, and SF_6 were less than 10% that of molecules smaller than nitrogen, and largely deviated from the predicted values by the Knudsen model based on helium permeance. This membrane seems to have few effective pores for the permeation of those large molecules, and it showed molecular sieving properties. Considering the sizes of N_2 (0.364 nm), CH_4 (0.38 nm), and C_3H_8 (0.43 nm), the mean effective micropore size of M-1 can be assumed to be around 0.4–0.5 nm. The permeance of SF_6 on M-2 was somewhat lower than the Knudsen permeance, and this membrane

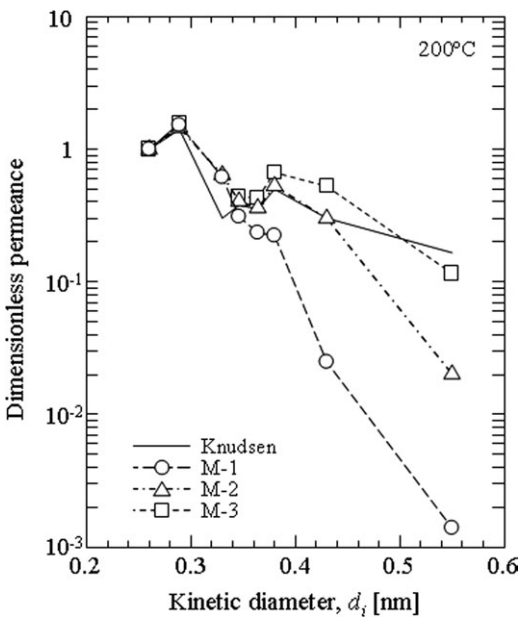

Figure 5. Gas molecular kinetic diameter dependency of normalized gas permeance at 200°C.

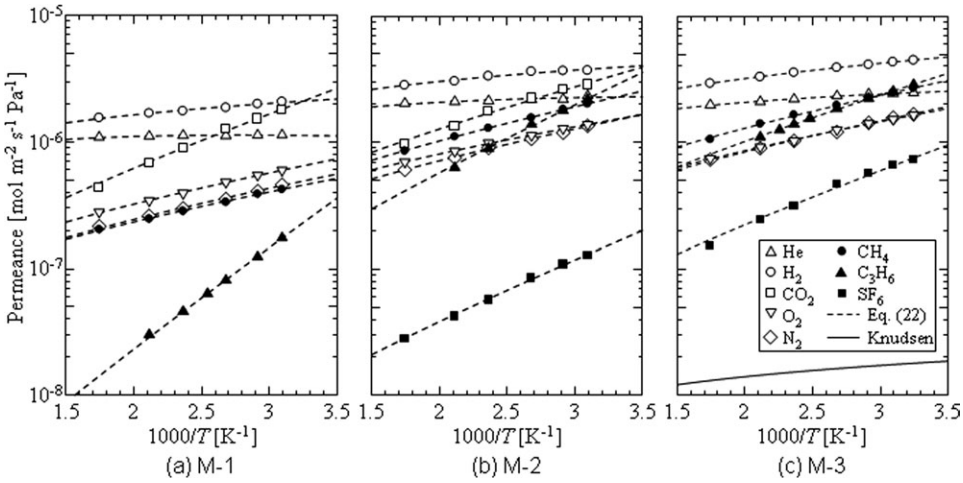

Figure 6. Temperature dependence of gas permeance for (a) M-1, (b) M-2, and (c) M-3 membranes in the temperature range of 35–300°C.

The solid curve in (c) indicates only the slope of the temperature dependence of arbitrary gas permeance, as predicted by the Knudsen diffusion model.

showed diminished molecular sieving performance compared to M-1. The M-2 membrane seemed to have larger pores than the M-1, at around 0.5–0.6 nm, given that the size of SF_6 is 0.55 nm. On the contrary, the permeance for SF_6 on M-3 showed good agreement with the Knudsen permeance, which indicated that this membrane had pores that were too large for the purpose of gas separation. CO_2 and C_3H_6 permeances were greater than the predicted Knudsen permeances on M-3. This might have been caused by a concentration enhancement in the micropores of these molecules due to the large affinity of CO_2 and C_3H_6 with the pore surface, which would lead to the so-called surface diffusion effect. The effective pore size of M-3 seems to be small enough for gas molecules to permeate though a pore by the Knudsen and surface diffusion mechanisms, but it was difficult for us to estimate the pore size of M-3 from the gas permeation data. We can only surmise that the pore size might have been greater than 0.55 nm.

The silica membranes used in this work had rather lower H_2/N_2 selectivity than reported hydrogen separation membranes by Nomura et al.[4] and Kanezashi and Asaeda.[5] M-1 and M-2, however, showed higher permselectivity than expected from the helium permeance-based Knudsen diffusion, as shown in Figure 5. For example, the observed permeance ratio of He/SF_6 at 200°C for M-1 was 790, and $He/C_3H_8 = 80$, which obviously indicated that there were very few pores with a size that was larger than the size of SF_6, 0.55 nm. For M-2, the He/SF_6 permeance ratio was 38 and was greater than the Knudsen selectivity of 7, while the permeance ratio of He/CH_4 was nearly equal to the Knudsen selectivity of 2. This membrane could be said to have moderate molecular permselectivity. On the other hand, for M-3, each dimensionless gas permeance showed good agreement with the predicted value by the Knudsen diffusion model, which suggested that the diameter of the micropores of M-3 was larger than 0.55 nm. The existence of pinholes and cracks were not clearly ruled out based on only the molecular size dependence of gas permeance. Therefore, the presented model was not verified with the gas permeance data of M-3. Concerning M-3, the present model was applied to estimate its pore size. In particular, for such a membrane as M-3, the proposed method for micropore size estimation by measuring the temperature dependency of gas permeance was expected to provide clues for the existence or nonexistence of pinholes.

Figure 6a–c show Arrhenius plots of gas permeances for M-1, 2, and 3, respectively. In general, amorphous silica membranes for hydrogen/methane separation have an active separation layer, a major part of which consisted of a silica polymer network, and the void size of the network was assumed to be around 0.3 nm.[7] Therefore, He (0.26 nm) and H_2 (0.289 nm) molecules permeated the network voids according to the activated diffusion mechanism. Because the molecular sieving effect surpassed the Knudsen diffusion effect for such membranes, the permeance of He, which has a smaller molecular size, was greater than that of the lighter, but larger, H_2, and the activation energy for the permeation of H_2 tended to be greater than that of He. On the contrary, all of the silica membranes, M-1, −2, and −3, used in this study showed greater permeance for the lighter H_2 than that for the heavier He. These silica membranes, with pore sizes greater than that of the natural silica polymer network voids of hydrogen separation membranes, were successfully prepared by controlling silica colloid size and coating times. The aggregate pores that originated from intercolloidal voids were assumed to effectively remain open for gas permeation even after calcination. The membranes M-3, −2, and −1 represented the order of gas permeance. M-1 showed the largest difference in permeance between gas species, which was consistent with the kinetic diameter dependency of gas permeance at 200°C, as shown in Figure 5. The temperature dependency of permeance, however, was strongly dependent on gas species, particularly for M-1. The inclinations for He, H_2, O_2, and N_2 were relatively small and were similar to that of the temperature dependency curve predicted by the Knudsen diffusion model. On the contrary, the inclinations for CO_2, C_3H_8, and SF_6 were obviously greater by comparison with those of other inorganic gases, and the permeances notably increased with decreasing temperature possibly due to a larger affinity to the pore surface, which could be explained by the so-called surface diffusion mechanism.

Because the temperature dependency of gas permeance depends on the gas species, the molecular diameter

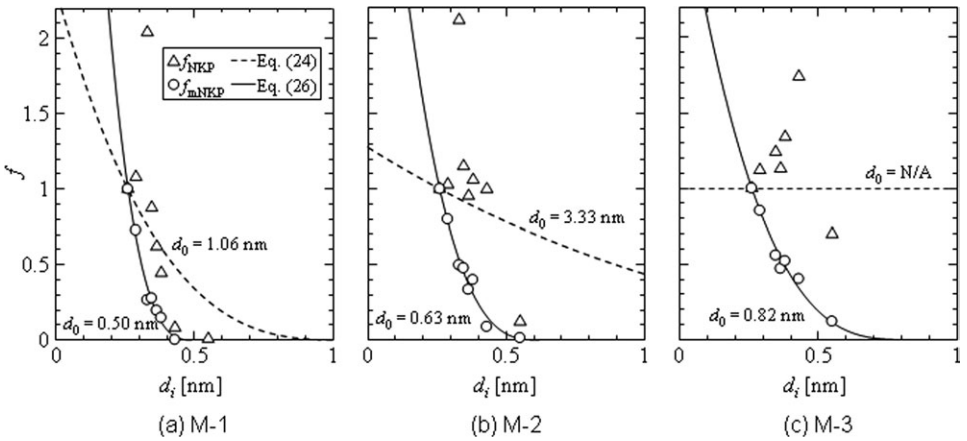

Figure 7. Comparison of the NKP-plot and the modified NKP-plot for (a) M-1, (b) M-2, and (c) M-3 membranes at 200°C.

dependencies of gas permeance are different at different temperatures. According to the gas permeation model described by Eq. 22, the difference in gas species dependency of temperature dependency of gas permeance becomes smaller with increasing temperature, and in that case, the gas permeance is assumed to mainly depend on molecular weight and size but less depend on $E_{P,i}$. Therefore, a molecular size dependency curve of gas permeance at a high temperature can give us a rough estimation of effective pore size for gas permeation. However, the previous NKP-plot, that neglects the difference in $E_{P,i}$ among different gas species, is not suitable for estimation of a unique micropore size when a significantly large temperature dependency of gas permeance can be observed. In this work, we tried to estimate an effective micropore size more accurately by the "modified NKP-plot" or "k_0-plot" by considering the difference in temperature dependency among several probe gas species.

The values of the adjusting parameters, $k_{0,i}$ and $E_{P,i}$, were obtained by using Eq. 22 to fit the temperature dependency of each gas permeance to a curve.

Figure 7 shows both the simple f_{NKP} defined by Eq. 24 and f_{mNKP} defined by Eq. 26, which is an f_{NKP} that has been modified using the $E_{P,i}$ of each gas, and using $E_{P,He}$ as $E_{P,S}$ plotted against the kinetic diameters. The gas permeance for each membrane at 200°C was adopted for the plot. The calculated curves of Eqs. (24) and (26) using the He diameter of 0.26 nm as d_S were also drawn to adjust the parameter d_0. The obtained values of d_0 are summarized in Table 4. In a previous paper,[24] an NKP-plot was constructed for BTESE membranes, and the observed temperature dependencies of gas permeance were relatively small. Because the absolute values of $E_{P,i}$ were small enough so as to be reasonably negligible, a normal NKP plot successfully had given the effective mean pore sizes for gas permeation. In this work, the estimated pore diameters, d_0, of silica membranes M-1 and −2 from Eq. 24 were 1.06 and 3.32 nm, respectively. These values of d_0 were not consistent with the molecular sieving performance of these membranes, as shown in Figure 5. For M-3, a usable pore size estimation from Eq. 24 was impossible. As shown in Figure 6 and Table 3, the observed temperature dependencies of gas permeance were dependent on gas species, and the difference in $E_{P,i}$ was evident. In this case, it was not suitable to estimate pore size from the normal NKP plot. However, clear correlations between f_{mNKP} and the kinetic diameter of permeating gas molecules were observed. The deviation of f_{mNKP} from unity increased as molecular size increased. The estimated pore diameters, d_0, of M-1, −2, and −3, using Eq. 26 were 0.50, 0.63, and 0.82, respectively, which was consistent with the roughly predicted pore size from the kinetic diameter dependencies of gas permeance shown in Figure 5.

The relationship between the values of the cubic root of $k_{0,i}$ and the kinetic molecular diameter of a gas molecule, i, were plotted in Figure 8 for M-1, −2, and −3. We observed a good linear correlation for all membranes, and Eq. 28 was successfully fitted to those curves by adjusting two parameters of k_0 and d_0. The obtained values of k_0 and d_0 are also summarized in Table 4. These adjusted values of d_0 for each membrane showed good agreement with those obtained in the mNKP plot shown in Figure 7. These results could be logical because both of the curve-fitting analyses in Figures 7 and 8 are based on the same gas permeation model equation of (22). We should note here that the value of the adjustable parameter k_0 has a physical meaning as defined by Eq. 15. That is, k_0 is proportional to the number of effective

Table 3. Adjusted values of $k_{0,i}$ and $E_{P,i}$ in Eq. (22) for M-1, −2 and −3

	M-1		M-2		M-3	
	$k_{0,i} \times 10^7$	$E_{P,i}$ (kJ/mol)	$k_{0,i} \times 10^7$	$E_{P,i}$ (kJ/mol)	$k_{0,i} \times 10^7$	$E_{P,i}$ (kJ/mol)
He	64.5	1.50	108	0.99	93.7	0.41
H_2	46.7	−0.06	87.7	−0.02	79.2	−0.64
CO_2	17.4	−6.52	55.4	−4.71	–	–
O_2	17.9	−3.02	51.6	−2.45	51.5	−2.72
N_2	12.6	−3.03	36.2	−3.13	43.4	−3.05
CH_4	9.55	−2.85	36.0	−2.85	48.0	−3.29
C_3H_8	0.118	−13.63	9.84	−8.59	38.0	−5.34
SF_6	–	–	1.50	−7.64	11.5	−6.51

Table 4. Estimated Values of d_0 and k_0 for M-1, −2 and −3

	d_0 (nm)				k_0 (nm^{-3})
	Figure 5	*NKP-plot*	*modified NKP-plot*	Figure 8	(Figure 8)
M-1	0.4–0.5	1.06	0.497	0.472	7.44×10^{-4}
M-2	0.5–0.6	3.33	0.628	0.625	2.19×10^{-4}
M-3	>0.55	N/A	0.823	0.852	4.36×10^{-5}

pores for gas permeation, and is inversely proportional to the membrane area, membrane thickness, and tortuosity.

The active separation layers of membranes M-1, −2, and −3 were prepared by controlling the sol colloidal size and coating times. As a result, both the pore diameter and the membrane thickness were assumed to be different for each membrane. Therefore, in a model calculation, if we suppose that the thicknesses of the separation layers, L, of membranes M-1, −2, and −3 would be 300, 200, and 100 nm, respectively, referring to a previously reported SEM image for the cross-section of a silica membrane,[5] the number of pores per membrane area, N_P/A_m, as calculated from k_0 would be 0.76, 0.15, and 0.015 nm^{-2}, respectively. M-3, which was prepared using relatively less coating time and a larger size of colloids, could have one 0.8 nm pore per area of 8×8 nm^2. This would be reasonable if the aggregated pore could be formed by coating silica colloids with sizes that were around 10–50 nm. By comparison, M-1 could have one 0.5 nm pore per area of 1.15×1.15 nm^2. The top layer of M-1 might be formed by a coating of very small colloids of less than 10 nm or silica polymers, and, therefore, this membrane could possess very small micropores very close to the native void size of a silica polymer network (0.3 nm). The above discussion of the membrane structures is only an example that was derived from the model calculation using assumptions, and there is no evidence for its accuracy. This shows, however, that the values of d_0 and k_0 obtained by the presented analysis procedure would give us useful information on the microporous structures of gas separation membranes by comprehensively comparing them with other information such as preparation procedures and conditions, direct observation results from an electron microscope, and gas permeation properties.

MD simulation

Figure 9 shows perspective views of three different virtual silica membrane models from the upstream side along with the direction of gas permeation. A different size of cylindrical penetrating pore was formed on each membrane model, which was perpendicular to the direction of permeation. Because the silica that formed the pore wall was made up of amorphous structures, the surface of the pore wall was not smooth and did not have a homogeneous convex and concave geometry according to molecular size. The pore shapes were not perfectly cylindrical, and the cross-section of the pore was distorted from that of a perfect circle.

The pore-size distribution of each model was calculated as follows.[7,34] First, the center part of a membrane, which included the penetrating pore, was divided into N small cubic bins each 0.017 nm in length. The volume of each small bin V_b, was 4.9×10^{-6} nm^3. The portions for pore size estimation were $1.1 \times 1.1 \times 2.053$ nm^3 for VM-1, $1.4 \times 1.4 \times 2.053$ nm^3 for VM-2, and $1.6 \times 1.6 \times 2.053$ nm^3 for VM-3. The largest diameter of a sphere, d_m, that could be settled on each grid point without overlapping atoms on the membrane was calculated and a list for d_m ($m = 1, 2, \ldots, N$) was prepared. The sizes of Si and O were 0.041 (Si), 0.27 (b-O), and 0.30 nm (nb-O). For each grid point i ($i = 1, 2, \ldots, N$), spheres to which the grid point belonged were checked, and the grid point i was assumed to be only a part of the largest sphere of d_0 among them. The largest sphere with a center grid point of i was not necessarily the largest sphere that included a grid point i. That is, each grid point may belong to another larger sphere. Finally, the number of grid points, n, for d_0 was counted as a function of d_0, and the void volume of a pore d_0 was estimated as $V = nV_b$. A schematic image of this "grid point in the L-sphere" calculation method is shown in Figure 10. This calculation method enabled us to estimate any small void size correctly by reduction to a bin size that was small enough. This calculation method would also be useful to estimate void volume distribution in denser polymer network structures. The calculated pore-size distributions of each of the membrane models, VM-1, −2, and −3 are shown in Figure 11. The location of the largest narrow peak indicates the representative pore size of the membrane. Most of the sizes of VM-1, −2, and −3 were 0.62, 0.91, and 1.13 nm, respectively. Despite a penetrating cylindrical form of the pore, the convex and concave geometry on the pore surface was well-reflected by the resultant broad pore-size distributions.

Figure 12 shows the observed density profiles of several virtual models of permeating gas species along the radial direction in a pore of VM-1 ($d_0 = 0.62$ nm) at a steady state. The profile reflects the existence region of molecules. Each density profile was normalized by the density of each gas molecule at the pore center. All molecules were localized at the pore center side, and their densities gradually decreased toward the pore wall. This means that the potential minimum caused by the pore wall was not located near the pore wall but around the pore center due to the overlapping effect in this subnanoscale small pore. He and Ne molecules with sizes that were relatively smaller were distributed in a wider region of the pore from the pore center to the neighborhood of the pore wall. On the contrary, the density profile narrowed as molecular size increased. This means that the effective pore diameter for gas transportation in a subnanoscale micropore significantly depends on the molecular size of a permeating gas molecule, as schematically shown in

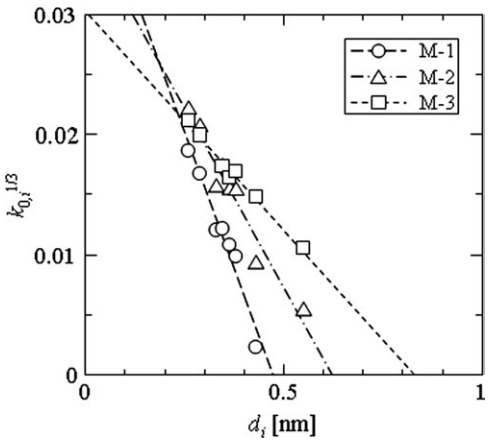

Figure 8. Relationship between the values of $k_{0,i}^{1/3}$ and the kinetic molecular diameter of gas molecule d_i.

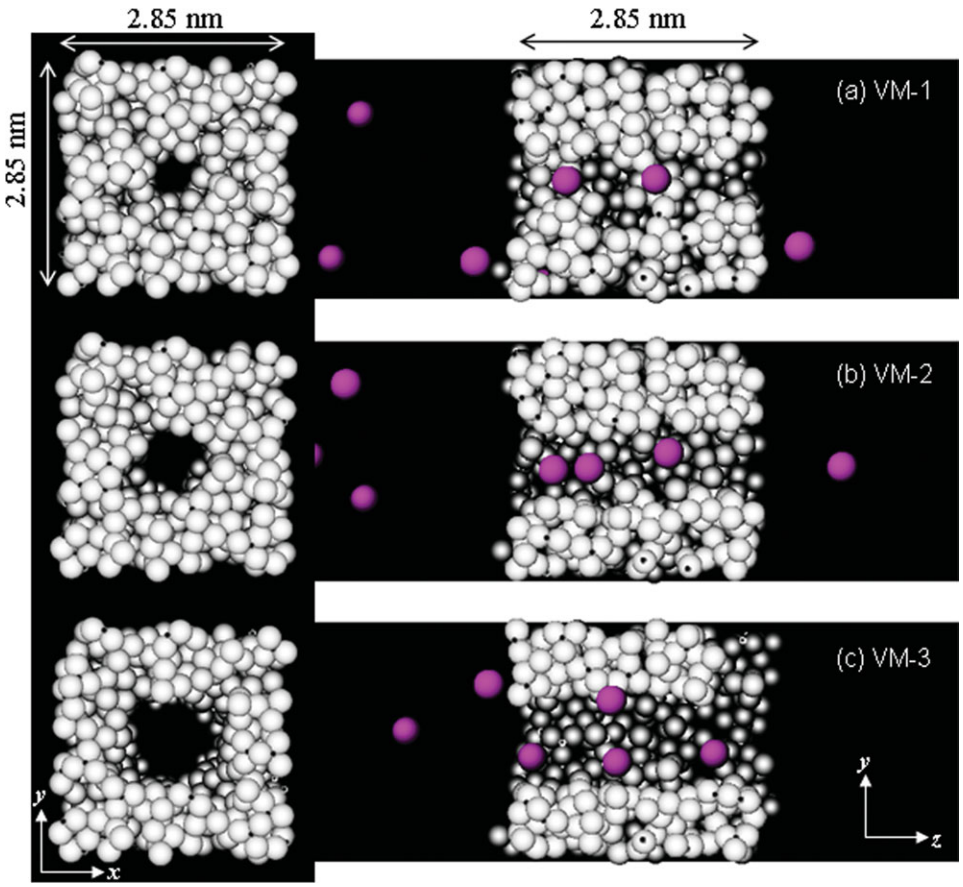

Figure 9. Front views of the membrane surface and cross-sectional views of the three virtual silica membranes, (a) VM-1, (b) VM-2, and (c) VM-3.

Cross-sectional views are snapshots of CH_4 permeation at 400°C. [Color figure can be viewed in the online issue, which is available at wileyonlinelibrary.com.]

Figure 1. It seems to be reasonable to assume that the effective pore diameter for molecular diffusion must be smaller than the actual pore size by nearly a size of permeating molecule.

Figure 13 shows the temperature dependency of the simulated permeance for VM-1, −2, and −3. The solid curves in the figure are fitted curves by Eq. 22, and the values of adjusted parameters $k_{0,i}$ and $E_{P,i}$ are summarized in Table 5. The observed gas permeances for VM-3, with the largest pore of the examined three models, were relatively high for the most part, and showed a temperature dependency that was similar to the predicted curve based on the Knudsen diffusion theory. The simulated gas permeance decreased with decreasing pore size on the order of VM-3, −2, and −1. Gas molecules with larger values for the ε parameter, with a larger affinity for the pore wall, showed a larger temperature dependency for permeance. The adjusted quantitative values for $k_{0,i}$ and $E_{P,i}$ well-reflected the effective porous structures for permeation and affinity of the pore surface, respectively.

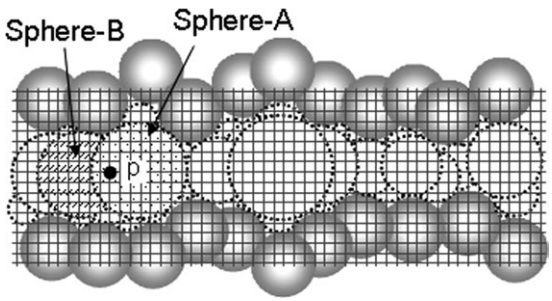

Figure 10. Schematic image of the "grid point in L-sphere" for pore size calculation (A point "p," which belongs to both the sphere-A and −B, is deemed to be not a part of sphere-B but a part of the larger sphere-A).

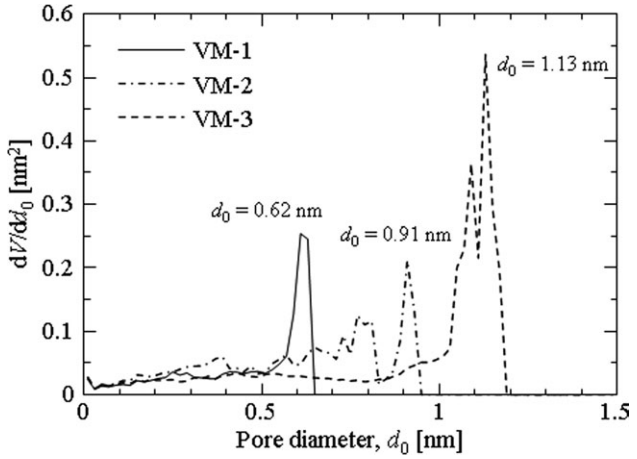

Figure 11. Pore-size distribution of virtual silica membranes.

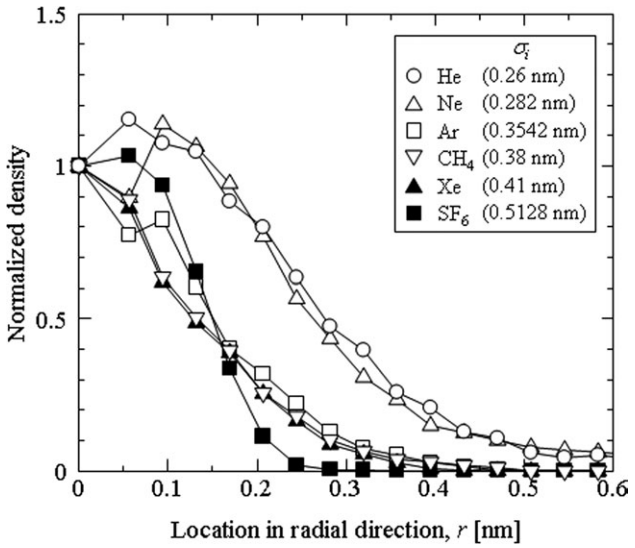

Figure 12. Density profile of permeating gas molecules along with the radial direction in the pore of VM-1.

The cubic root of $k_{0,i}$ was plotted against the size parameter σ of the LJ potential for VM-1, −2, and −3, as shown in Figure 14. A good linear correlation was found among the three membrane models, which all fit well to Eq. 28. The estimated values for k_0 and d_0 are summarized in Table 6. The values of d_0 for VM-1 and VM-2 showed good agreement with the real pore sizes indicated as the major peaks in Figure 11. For VM-3, however, the estimated value of d_0 from Figure 14 was obviously greater than the real pore size shown in Figure 11. It is possible that gas permeation mechanisms could be well-described by Eq. 22 for micropores smaller than 1 nm, while, for larger pores, gas permeation phenomena are often described by the cooperative bimodal permeation mechanism of Knudsen diffusion around a pore center and surface diffusion over the pore wall. Therefore, as Eq. 22 supposes a monomodal gas permeation mechanism under conditions of homogeneity in a radial direction, it would fail to describe the gas permeation properties of larger pores.

Table 5. Adjusted Values of $k_{0,i}$ and $E_{P,i}$ in Eq. 22 for VM-1, -2 and -3

	VM-1		VM-2		VM-3	
	$k_{0,i} \times 10^4$	$E_{P,i}$ (kJ/mol)	$k_{0,i} \times 10^4$	$E_{P,i}$ (kJ/mol)	$k_{0,i} \times 10^4$	$E_{P,i}$ (kJ/mol)
He	30.5	−0.04	79.8	−0.46	191	−0.43
Ne	29.5	−0.55	70.0	−1.22	202	−0.44
Ar	13.1	−6.02	60.2	−3.48	155	−2.50
CH_4	13.8	−7.57	51.1	−5.27	135	−3.48
Xe	11.8	−10.82	54.5	−6.53	137	−4.64
SF_6	1.79	−19.07	15.8	−14.48	127	−6.46

The two solid lines in Figure 14 indicate the calculated values of $k_{0,i}$ from Eqs. (15) and (28) with $N = 1$, A_m, = 8.14 nm^2, $L = 2.85$ nm, and $\tau = 1$, which are preset values of virtual membranes for both VM-1 ($d_0 = 0.62$ nm) and VM-2 (0.91 nm). Unfortunately, the qualitative agreement of the theoretical calculation lines with the simulation results was not perfect. This could be due to a deviation in the pore shapes from a perfect cylinder, which could have been caused by surface roughness. The value of d_0 used for the calculation was representative of a pore size as estimated from the peak in the pore-size distribution in Figure 11. Despite the above slight disagreements, however, the slopes of the two fitted curves for VM-1 and VM-2 in Figure 14 are obviously identical and agree with the slopes of the theoretical lines. This would suggest the adequacy of the presented gas permeation model as the slope k_0 as defined by Eq. 15 depends only on the membrane porous structures such as N_P, A_m, τ, and L, which were identically set for VM-1 and VM-2.

DDR zeolite membrane

To examine the adequacy of the gas permeation model and pore size estimation method based on Eq. 22, we investigated the relationship between $k_0^{1/3}$ and d_i for previously reported gas permeation data on a DDR zeolite membrane.[36] A DDR-type zeolite membrane has a homogeneous porous structure of 0.36 × 0.44 nm^2. A DDR membrane is expected to be effective for CO_2/CH_4 separation, and the established

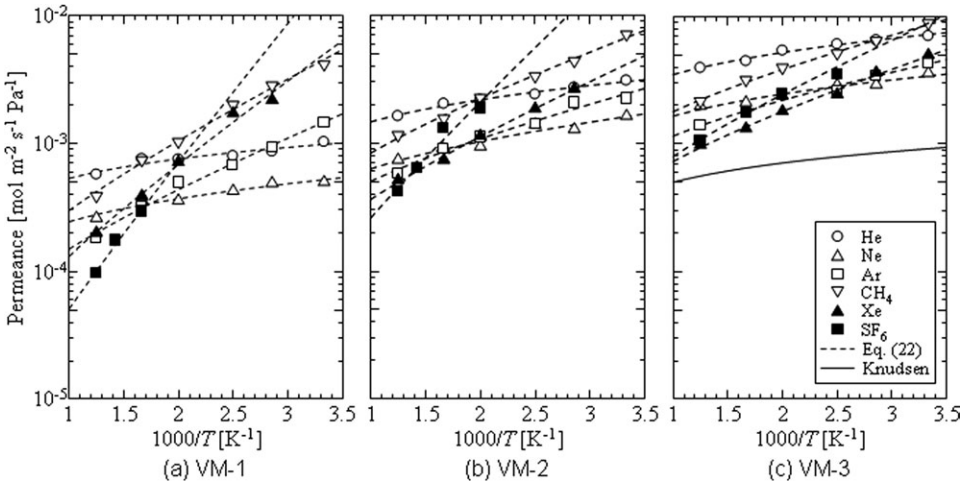

Figure 13. Temperature dependence of gas permeance for (a) VM-1, (b) VM-2, and (c) VM-3 membranes in the temperature range of 300–800 K.

The solid curve in (c) indicates only the slope of a temperature dependence of arbitrary gas permeance, as predicted by the Knudsen diffusion model.

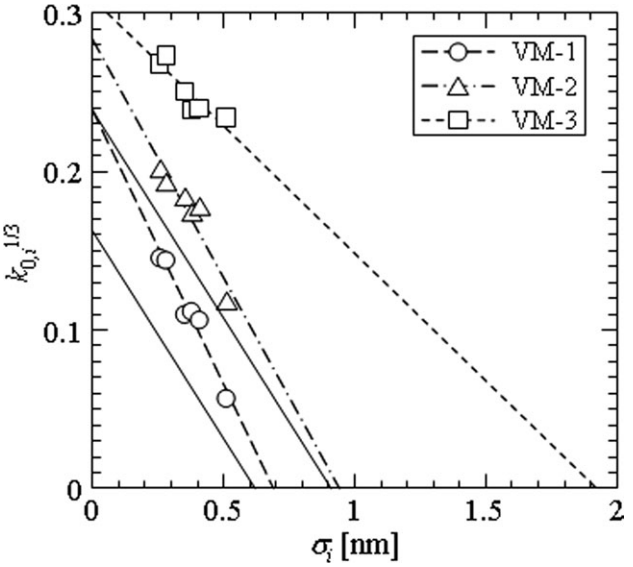

Figure 14. Relationship between the values of $k_{0,i}^{1/3}$ and σ_i parameter of the LJ potential for VM-1, -2, and -3.

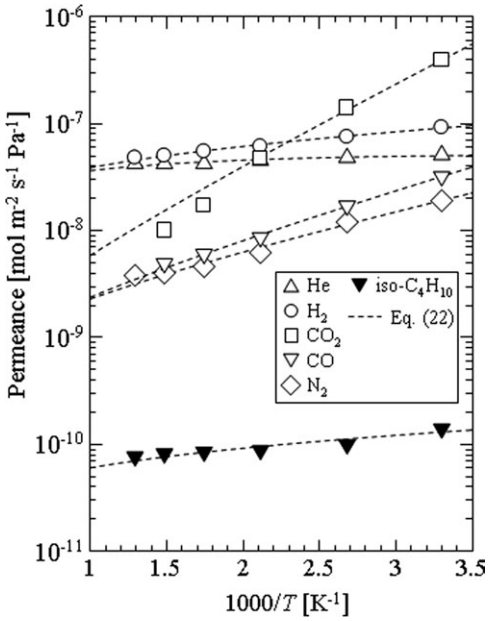

Figure 15. Temperature dependence of gas permeance for a reported DDR zeolite membrane in the temperature range of 30–500°C.

pore size seems to be suitable for verification of the presented method in this study. Figure 15 shows the Arrhenius plots of gas permeance for a DDR membrane as reported by Bergh et al.[36] The gas permeances of He and H_2 showed a Knudsen diffusion-type temperature dependency, whereas those of CO_2 and CO showed temperature dependence that was larger than the Knudsen's, but with a so-called surface diffusion tendency. However, the temperature dependency of gas permeance for i-C_4H_{10}, with a molecular size that was larger than the others, was expected to have a greater interaction with the pore surface, but was unexpectedly small and was the same as those of a Knudsen diffusion.

The values obtained for $k_{0,i}$ and $E_{P,i}$ by fitting Eq. 22 to those data are summarized in Table 7, and the relationship between $k_{0,i}^{1/3}$, and the d_i for this DDR membrane, is plotted in Figure 16. A good linear correlation was seen for molecules from He (0.26 nm) to CO (0.376 nm). For the permeation of these molecules, the adjusted value of d_0 from the d_i-intercept was 0.44 nm. When a linear line was drawn only for the three points corresponding to He, H_2, and CO_2, $d_0 =$ 0.39 nm, which seemed an adequate value for the micropore size of a DDR zeolite crystal. The plotted point for i-C_4H_{10}, however, evidently deviated from these two lines. Because the d_i-intercept of a fitted line using the four plotted points of CO_2, N_2, CO, and i-C_4H_{10} resulted in a $d_0 > 0.6$ nm, the observed gas permeances for these gases were supposed to have included the contribution of permeation through larger pores such as the slight remainders of the crystalline boundaries. This conjecture seems reasonable because a low, but detectable, i-C_4H_{10} permeance was observed despite the fact that the size of i-C_4H_{10} was 0.5 nm, so it naturally could not permeate the native crystalline pores of DDR zeolite. The d_0 values, however, that were obtained from the $k_{0,i}$ of smaller molecules, which can permeate zeolite crystalline pores, showed good agreement with the size of DDR zeolite native pores. Therefore, these smaller molecules might prevail as they are transported through the small crystalline pores. Assuming that $\tau = 1.41$ and $L = 2000$ nm, as in the example of a model calculation, the estimated values for the number density of a pore, N_P/A_m, as calculated by Eq. 15, showed a distribution that ranged from 0.76 to 0.26 nm^{-2} for $d_0 =$ 0.39 − 0.44 nm, as shown in Table 8. This high density of pores would be true of zeolite native pores. A relationship between $k_{0,i}^{1/3}$ and d_i should form one linear line for microporous membranes composed of uniform pores, while multiple lines or a curved line would be observed for a pore-size distribution. In the case of the DDR zeolite membrane, Figure 16 reflects the distinct bimodal porous structure of the membrane composed of zeolite crystalline pores occupying a major part of the membrane and a few crystalline boundaries. To the contrary, amorphous silica membranes were supposed to have a monomodal, but rather broad, pore-size distribution with larger pores, and, therefore, strict multiple linear lines were faintly observed as one of the limitations of accuracy in Figure 8. Therefore, one linear line was drawn as the representative mean pore size of a membrane.

Table 6. Estimated Values of d_0 and k_0 for VM-1, -2, and -3

	d_0 (nm)		k_0 (nm^{-3})
	Figure 11	k_0-plot (Figure 14)	(Figure 14)
VM-1	0.620	0.690	1.36×10^{-2}
VM-2	0.910	0.942	2.27×10^{-2}
VM-3	1.13	1.92	2.95×10^{-2}

Table 7. Adjusted Values of $k_{0,i}$ and $E_{P,i}$ in Eq. (22) for a DDR Zeolite Membranes

	$k_{0,i} \times 10^7$	$E_{P,i}$ (kJ/mol)
He	2.36	1.00
H_2	1.41	−0.93
CO_2	0.232	−13.05
N_2	0.180	−5.51
CO	0.152	−7.24
iso—C_4H_{10}	0.0124	−0.62

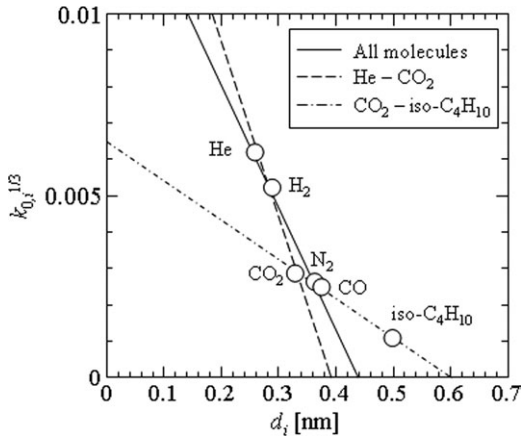

Figure 16. Relationship between the values of $k_{0,i}^{1/3}$ and the kinetic molecular diameter of gas molecule d_i for a reported DDR zeolite membrane.

Conclusions

A simple method that uses temperature dependency to estimate an effective micropore size for gas permeation was proposed by considering the molecular size of permeating gases based on the usual GT model for gas transport phenomena in the micropores of porous membranes. This method was applied to molecular sieving microporous silica membranes to estimate the mean pore sizes that would be effective for gas permeation. Taking into account the effect on gas permeation properties of the interaction of gas molecules with the pore wall could result in a better estimation for reasonable micropore sizes of microporous silica membranes compared with the past NKP method. MD simulations of gas permeation through virtual silica membranes, using previous measurements for pore sizes, were also carried out to analyze simulated gas permeation properties on a molecular scale. The effective diffusion lengths of micropores were distinguishable for several gas molecules possibly due to the differences in their molecular sizes, which indicated that the gas-state permeance of subnanoscale pores was affected by gas molecular size. The pore sizes of less than 1 nm for the virtual membranes were reliably estimated using the present method. For a pore model membrane with pore size greater than 1 nm, however, the calculated pore size was overestimated. The reason for the failure of the present method in estimating large pores is yet to be examined in detail. With a larger pore, the effect of a difference in gas molecular size on effective diffusion length might be relatively reduced in comparison with the large pore size, and the significant localization of gas molecules in the vicinity of the pore surface would have an important role in deciding the gas permeation characteristics. The present method could successfully give a reasonable native crystalline pore size of DDR zeolite through application to reported gas permeance data for a DDR zeolite membrane.

Table 8. Estimated values of d_0, k_0 and the number density of pore, N_P/A_m for a DDR zeolite membrane

	k_0-plot (Figure 16)			Native pore size of DDR zeolite
	All molecules	He—CO_2	CO_2—iso—C_4H_{10}	
d_0 (nm)	0.439	0.392	>0.6	0.36 × 0.44
$k_0 \times 10^4$ (nm^{-3})	0.378	1.12	(0.0126)	
N_P/A_m (nm^{-2})	0.256*	0.756*	(0.00850*)	

*$\tau = 1.41$, $L = 2000$ nm

The past NKP method enabled us to estimate the mean micropore sizes of membranes that had apparently little interaction with permeating gas molecules from a kinetic diameter dependency of gas permeance at a temperature that was as high as possible. However, silica and zeolite membranes can have a significant interaction with gas molecules and show a significant temperature dependency for permeance, and the contribution of $E_{P,i}$ in Eq. 22 should understandably never be ignored. Therefore, when estimating micropore size using the effect of gas molecular size on permeance, it is important to know the value of $E_{P,i}$ from gas permeance data at different temperatures. It is desirable to measure the permeance under conditions where a Henry-type adsorption and gas-state permeation occur to satisfy Eq. 22 at low pressures and high temperatures. Attention should also be paid to the meaning of another parameter, $k_{0,i}$, in Eq. 22. Because $k_{0,i}$ represents not only micropore size and gas molecular size but also the density of pores, the membrane thickness, and tortuosity, a detailed analysis of either $k_{0,i}$ or k_0 is expected to provide important information on the microporous structures of membranes.

Notation

A_0 = native cross-sectional area of pore, m^2
A_e = effective cross-sectional area of pore, m^2
A_m = membrane surface area, m^2
B = mobility, mol m^2 J^{-1} s^{-1}
c = gas concentration, mol m^{-3}
c_b = gas concentration in bulk phase, mol m^{-3}
d_0 = native pore diameter, m
d_e = effective pore diameter, m
d_i = kinetic diameter of i-th component, m
D = Fickian diffusivity, m^2 s^{-1}
D' = thermodynamic corrected diffusion coefficient, m^2 s^{-1}
$E(r_{ij})$ = Lennard-Jones potential energy for the i-th molecule, which is r_{ij} away from the j-th molecule, J
$E_{act,i}$ = activation energy for the permeation of the i-th component, J mol^{-1}
$E_{att,i}$ = attractive potential energy for the i-th component, J mol^{-1}
$E_{P,i}$ = summation of $E_{act,i}$ and $E_{att,i}$ for the i-th component, J mol^{-1}
$E_{P,S}$ = $E_{P,i}$ of the standard component, J mol^{-1}
f = frequency of gas molecular generation on a control plane, s^{-1}
f_{iNKP} = ideal normalized Knudsen-based permeance, dimensionless
f_{mNKP} = modified normalized Knudsen-based permeance, dimensionless
f_{NKP} = normalized Knudsen-based permeance, dimensionless
k_B = Boltzmann constant, J K^{-1}
k_0 = structural constant given by Eq. 15, m^{-3}
$k_{0,i}$ = permeation constant for the i-th component given by Eq. 29, dimensionless
L = membrane thickness (diffusion length in the direction of permeation), m
J = diffusive flux, mol m^{-2} s^{-1}
m = molecular weight, kg
M = molar weight, kg mol^{-1}
M_i = molar weight of the i-th component, kg mol^{-1}
M_S = molar weight of the standard component, kg mol^{-1}
N_P = the number of pores, dimensionless
p = pressure, Pa
p_1 = feed side pressure, Pa
p_2 = permeate side pressure, Pa
P = permeability, mol m Pa^{-1} m^2 s^{-1}
P_{cK} = concentrated Knudsen permeability, mol m Pa^{-1} m^2 s^{-1}
P_{cKL} = concentrated Knudsen permeance, mol Pa^{-1} m^2 s^{-1}
P_i = permeance of i-th component, mol Pa^{-1} m^2 s^{-1}
P_{iKL} = ideal Knudsen permeance, mol Pa^{-1} m^2 s^{-1}
P_S = permeance of standard component, mol Pa^{-1} m^2 s^{-1}
P_K = Knudsen permeability, mol m Pa^{-1} m^2 s^{-1}

P_{KL} = Knudsen permeance, mol Pa^{-1} m^2 s^{-1}
r_{ij} = distance between the i-th and j-th molecule, m
R = gas constant, J mol^{-1} K^{-1}
S = area of control plane, m^2
T = absolute temperature, K
z = position along with the direction of permeation in a pore, m

Greek letters

ε = porosity, dimensionless
ε_{ij} = geometric mean of the LJ energy parameter for i-th and j-th molecule, J
μ = chemical potential, J mol^{-1}
ρ = moving probability in a 3-D space, dimensionless
σ_{ij} = arithmetic mean of the LJ size parameter for the i-th and j-th molecule, m
τ = tortuosity, dimensionless

Literature Cited

1. Gavalas GR, Megiris CE, Nam SW. Deposition of H_2-permselective SiO_2 films. *Chem Eng Sci*. 1989;44:1829–1835.
2. de Lange RSA, Keizer K, Burggraaf AJ. Aging and stability of microporous sol-gel-modified ceramic membranes. *Ind Eng Chem Res*. 1995;34:3838–3847.
3. Lee D, Oyama ST. Gas permeation characteristics of a hydrogen selective supported silica membrane. *J Membr Sci*. 2002;210:291–306.
4. Nomura M, Ono K, Gopalakrishnan S, Sugawara T, Nakao S. Preparation of a stable silica membrane by a counter diffusion chemical vapor deposition method. *J Membr Sci*. 2005;251:151–158.
5. Kanezashi M, Asaeda M. Hydrogen permeation characteristics and stability of Ni-doped silica membranes in steam at high temperature. *J Membr Sci*. 2006;271:86–93.
6. Igi R, Yoshioka T, Ikuhara YH, Iwamoto Y, Tsuru T. Characterization of Co-doped silica for improved hydrothermal stability and application to hydrogen separation membranes at high temperatures. *J Am Ceram Soc*. 2008;91:2975–2981.
7. Yoshioka T, Tsuru T, Asaeda M. Molecular dynamics study of gas permeation through amorphous silica network and inter-particle pores on microporous silica membranes. *Mol Phys*. 2004;102:191–202.
8. Xiao J, Wei J. Diffusion mechanism of hydrocarbons in zeolites-I. Theory. *Chem Eng Sci*. 1992;47:1123–1141.
9. Shackelford JF, Studt PL, Fulrath RM. Solubility of gases in glass. Part II. He, Ne, and H_2 in fused silica. *J Appl Phys*. 1972;43:1619–1626.
10. Masaryk JS, Fulrath RM, Diffusivity of helium in fused silica, *J Chem Phys*. 1973;59:1198–1202.
11. Yoshioka T, Nakanishi E, Tsuru T, Asaeda M. Experimental study of gas permeation through microporous silica membranes. *AIChE J*. 2001;47:2052–2063.
12. Li S, Falconer JL, Noble RD. SAPO-34 membranes for CO_2/CH_4 separation. *J Membr Sci*. 2004;241:121–135.
13. Carreon MA, Li S, Falconer JL, Noble RD. SAPO-34 seeds and membranes prepared using multiple structure directing agents. *Adv Mater*. 2008;20:729–732.
14. Tomita T, Nakayama K, Sakai H, Gas separation characteristics of DDR type zeolite membrane. *Micropor Mesopor Mater*. 2004;68:71–75.
15. van den Bergh J, Zhu W, Gascon J, Moulijn JA, Kapteijn F. Separation and permeation characteristics of a DD3R zeolite membrane. *J Membr Sci*. 2008;316:35–45.
16. Ohta Y, Akamatsu K, Sugawara T, Nakao A, Miyoshi A, Nakao S. Development of pore size-controlled silica membranes for gas separation by chemical vapor deposition. *J Membr Sci*. 2008;315:93–99.
17. Kanezashi M, Yada K, Yoshioka T, Tsuru T. Design of silica networks for development of highly permeable hydrogen separation membranes with hydrothermal stability. *J Am Chem Soc*. 2009;131:414–415.
18. Kanezashi M, Yada K, Yoshioka T, Tsuru T. Organic-inorganic hybrid silica membranes with controlled silica network size: Preparation and gas permeation characteristics. *J Membr Sci*. 2010;348:310–318.
19. Chang K, Yoshioka T, Kanezashi M, Tsuru T, Tung K. A molecular dynamics simulation of a homogeneous organic-inorganic hybrid silica membrane. *Chem Commun*. 2010;46:9140–9142.
20. Kanezashi M, Kawano M, Yoshioka T, Tsuru T. Organic-inorganic hybrid silica membranes with controlled silica network size for propylene/propane separation. *Ind Eng Chem Res*. 2012;51:944–953.
21. Duke MC, Pas SJ, Hill AJ, Lin YS, da Costa JC. Exposing the molecular sieving architecture of amorphous silica using positron annihilation spectroscopy. *Adv Funct Mater*. 2008;18:3818–3826.
22. Tsuru T, Hino T, Yoshioka T, Asaeda M. Permporometry characterization of microporous ceramic membranes. *J Membr Sci*. 2001;186:257–265.
23. Tsuru T, Takata Y, Kondo H, Hirano F, Yoshioka T, Asaeda M. Characterization of sol-gel derived membranes and zeolite membranes by nanopermporometry. *Sep Purif Technol*. 2003;32:23–27.
24. Lee HR, Kanezashi M, Shimomura Y, Yoshioka T, Tsuru T. Evaluation and fabrication of pore-size-tuned silica membranes with tetraethoxydimethyl disiloxane for gas separation. *AIChE J*. 2011;57:2755–2765.
25. Shelekhin AB, Dixon AG, Ma YH. Theory of gas diffusion and permeation in inorganic molecular-sieve membranes. *AIChE J*. 1995;41:58–67.
26. Ferry JD. Ultrafilter membranes and ultrafiltration. *Chem Rev*. 1936;18:373–455.
27. Burggraaf AJ. Single gas permeation of thin zeolite (MFI) membranes: theory and analysis of experimental observations. *J Membr Sci*. 1999;155:45–65.
28. Breck DW. *Zeolite Molecular Sieves: Structure, Chemistry, and Use*. New York: Wiley, 1974:636.
29. Feuston BP, Garofalini SH. Empirical three-body potential for vitreous silica. *J Chem Phys*. 1988;89:5818–5824.
30. Yoshioka T, Tsuru T, Asaeda M. Molecular dynamics studies on gas permeation properties through microporous silica membranes. *Sep Purif Technol*. 2001;25:441–449.
31. Yoshioka T, Asaeda M, Tsuru T. A molecular dynamics simulation of pressure-driven gas permeation in a micropore potential field on silica membranes. *J Membr Sci*. 2007;293:81–93.
32. Miyahara M, Yoshioka T, Okazaki M. Determination of adsorption equilibria in pores by molecular dynamics in a unit cell with imaginary gas phase. *J Chem Phys*. 1997;106:8124–8134.
33. Ford DM, Glandt ED. Molecular simulation study of the surface barrier effect. Dilute gas limit. *J Phys Chem*. 1995;99:11543–11549.
34. Pohl PI, Heffelfinger GS. Massively parallel molecular dynamics simulation of gas permeation across porous silica membranes. *J Membr Sci*. 1999, 155:1–7.
35. Steele WA, *The interaction of gases with solid surfaces*. In: Everett DH, editor. *Properties of Interfaces*, *Chapter 2*. Oxford: Pergamon Press, 1974.
36. van den Bergh J, Tihaya A, Kapteijn F. High temperature permeation and separation characteristics of an all-silica DDR zeolite membrane. *Micropor Mesopor Mater*. 2010;132:137–147.

Manuscript received May 30, 2012, and revision received Nov. 1, 2012.